IOPscience iopscience.iop.org

Home Search Collections Journals About Contact us My IOPscience

Magnetic and transport properties of lanthanide rhenates $Ln_4Re_6O_{19}$ (Ln = La,Pr,Nd)

This article has been downloaded from IOPscience. Please scroll down to see the full text article.

2006 J. Phys.: Condens. Matter 18 9031

(http://iopscience.iop.org/0953-8984/18/39/030)

View the table of contents for this issue, or go to the journal homepage for more

Download details:
IP Address: 129.252.86.83
The article was downloaded on 28/05/2010 at 14:09

Please note that terms and conditions apply.

INSTITUTE OF PHYSICS PUBLISHING JOURNAL OF PHYSICS: CONDENSED MATTER

J. Phys.: Condens. Matter **18** (2006) 9031–9046 doi:10.1088/0953-8984/18/39/030

Magnetic and transport properties of lanthanide rhenates $Ln_4Re_6O_{19}$ (Ln = La, Pr, Nd)

Ai Sasaki, Makoto Wakeshima and Yukio Hinatsu

Division of Chemistry, Graduate School of Science, Hokkaido University, Sapporo 060-0810, Japan

Received 31 July 2006
Published 15 September 2006
Online at stacks.iop.org/JPhysCM/18/9031

Abstract

The crystal structures and magnetic properties of $Ln_4Re_6O_{19}$ (Ln = La, Pr, Nd) are reported. They crystallize in a cubic structure with space group $I23$ and have a three-dimensional network of Re_2O_{10} dimers consisting of two edge-sharing ReO_6 octahedra. Measurements of the magnetic susceptibility, specific heat, and electrical resistivity for $Ln_4Re_6O_{19}$ and the calculation of the electronic structure for $La_4Re_6O_{19}$ reveal that the 5d electrons of the Re ion are delocalized and that these compounds are metallic. For $Ln_4Re_6O_{19}$ (Ln = Pr, Nd), a Schottky-type specific heat anomaly is observed at 2 K for Ln = Pr and 5 K for Ln = Nd, which is due to the short-range magnetic orderings in the Ln_4O tetrahedral cluster. Furthermore, for the $Nd_4Re_6O_{19}$ compound, the long-range magnetic ordering via conduction electrons is found at 0.45 K.

(Some figures in this article are in colour only in the electronic version)

1. Introduction

Many ternary oxides containing both the lanthanide element and 4d(5d) transition metal show exotic electronic properties. Pyrochlore-type oxides $Ln_2M_2O_7$ (Ln = lanthanide; M = Mo, Ru, Ir) exhibit a spin-glass behaviour caused by their geometrically frustrated systems [1–7]. The magnetic behaviour of weberite-type compounds Ln_3MO_7 (Ln = lanthanide; M = Mo, Ru, Re, Os, Ir) at low temperatures is complicated due to cooperative magnetic orderings of lanthanide and transition metal ions [8–14]. Recently, the magnetic susceptibility, electrical conductivity, and specific heats for the $KSbO_3$-related-type lanthanum ruthenate $La_4Ru_6O_{19}$ were investigated and this compound was reported to have a non-Fermi-liquid characteristic [15] such as a heavy fermion which is often observed in lanthanide and actinide intermetallic compounds. This unique phenomenon can be explained by hybridization of Ru d-orbitals due to short Ru–Ru bondings in $La_4Ru_6O_{19}$ [16].

We focus our attention on the electrical and magnetic properties of the lanthanide rhenates $Ln_4Re_6O_{19}$ (Ln = La–Nd) which are isostructural with $La_4Ru_6O_{19}$. The $Ln_4Re_6O_{19}$ compounds have a cubic structure with space group $I23$ [17, 18]. The Re cation is octahedrally coordinated by six oxide ions and two ReO_6 octahedra share one edge forming a Re_2O_{10}

 © 2006 IOP Publishing Ltd Printed in the UK

dimer. These Re_2O_{10} dimers share corners, thus forming a three-dimensional network. A lanthanide ion in this three-dimensional network is surrounded by ten oxide ions. As for their physical properties, the $La_4Re_6O_{19}$ compound has been reported to show metallic electrical conductivity [19]. The magnetic susceptibilities of $Ln_4Re_6O_{19}$ (Ln = Ce, Pr, Nd) are paramagnetic above the liquid-nitrogen temperature [18].

These compounds are expected to show interesting electrical conductivities because the rhenium ion is in the mixed valence state (+4.33). Furthermore, for $Ln_4Re_6O_{19}$ containing the magnetic Pr^{3+} or Nd^{3+} ions, magnetic interactions between the localized 4f electrons and the delocalized Re 5d electrons may cause a unique magnetic behaviour. In this study, we have investigated the electrical and magnetic properties of $Ln_4Re_6O_{19}$ (Ln = La–Nd) through electrical conductivity, magnetic susceptibility, and specific heat measurements.

2. Experimental details

Lanthanide oxides (Pr_6O_{11}, Ln_2O_3; Ln = La, Nd) and rhenium oxides (ReO_2, Re_2O_7) were used as starting materials. In order to prepare La and Nd compounds, it was necessary to prepare Ln_3ReO_8 (Ln = La, Nd) in advance. Ln_3ReO_8 compounds were prepared by the following technique. Ln_2O_3 (Ln = La, Nd) and Re_2O_7 were weighed in appropriate metal ratios and dissolved in dilute nitric acid (∼1 M). The excess nitric acid was removed by gentle heating and the remaining powders were heated at 600 °C for 3 h. After cooling to room temperature, the samples were ground into powders, pressed into pellets, and then the pellets were reheated at 1000 °C for 6 h in air, with a intermediate regrinding. For the preparation of the Ln = Pr compound, Pr_6O_{11} was reduced to Pr_2O_3 in a flowing H_2:Ar = 1:9 atmosphere at 900 °C for 3 h.

$Ln_4Re_6O_{19}$ (Ln = La, Pr, Nd) compounds were synthesized by heating mixtures of Ln_3ReO_8 (Ln = La, Nd) or Pr_2O_3 and 10–15% excess ReO_2. The mixtures were ground in an agate mortar, pressed into pellets and then sealed in an evacuated platinum tube. They were heated at 1000 °C for Ln = La, at 1050 °C for Ln = Pr and at 900 °C for Ln = Nd for 24–60 h, with several intermediate regrindings.

X-ray powder diffraction measurements were performed with Cu Kα radiation on a Rigaku MultiFlex diffractometer equipped with a curved graphite monochromator. Intensity data were collected by step scanning in the range between 10° and 120° at intervals of 0.02°. The structure and lattice parameters were refined with the Rietveld program RIETAN 2000 [20].

The temperature dependence of the magnetic susceptibility was measured in an applied field of 0.1 T over the temperature range 1.8 K $\leqslant T \leqslant$ 300 K, using a SQUID magnetometer (Quantum Design, MPMS-5S).

Specific heat measurements were performed using a relaxation technique by a commercial heat capacity measuring system (Quantum Design, PPMS) in zero field and in an applied field of 4 and 8 T over the temperature range 0.35–400 K. The sample in the form of a pellet was mounted on a thin alumina plate with N- and H-Apiezon grease for better thermal contact.

Electrical resistivities were measured using a dc four-probe technique with the physical property measurement system (Quantum Design, PPMS model). The sample was sintered, and then cut into a piece approximately 6 mm × 2 mm × 1 mm in size. Four gold wire electrodes were attached to the sample with silver paste. The measurements were performed in an applied field of 0–8 T over the temperature range 0.35–400 K.

The calculations of the electronic structure and the density of states (DOS) were performed using the WIEN2k program [21]. This program employs the full potential linearized augmented plane wave + local orbitals (FP-LAPW + lo) method based on the density functional theory (DFT) with the generalized gradient approximation (GGA).

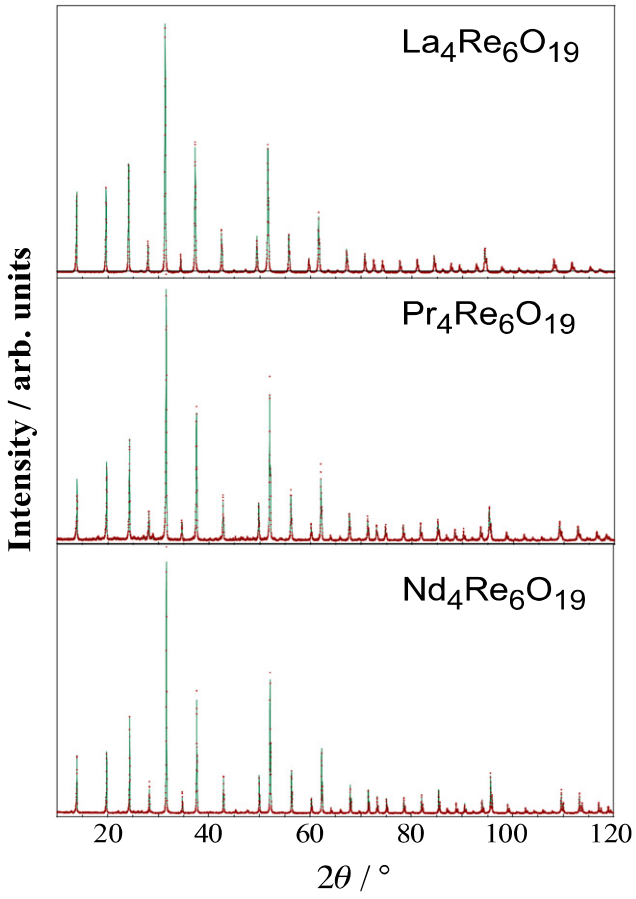

Figure 1. X-ray diffraction profiles for $La_4Re_6O_{19}$, $Pr_4Re_6O_{19}$ and $Nd_4Re_6O_{19}$. The calculated and observed diffraction profiles are shown by the solid line and cross markers, respectively.

3. Results and discussion

3.1. Sample preparation and crystal structure

We have prepared ternary lanthanide rhenates $Ln_4Re_6O_{19}$ (Ln = La, Pr, Nd). Figure 1 shows the calculated and observed x-ray diffraction profiles of these compounds measured at room temperature. Attempts at preparing $Ce_4Re_6O_{19}$ were unsuccessful owing to the chemical stability of the starting material CeO_2. A small amount of unidentified impurities were contained in the Pr and Nd samples.

The x-ray diffraction data of the $Ln_4Re_6O_{19}$ (Ln = La, Pr, Nd) phases could be indexed in a cubic unit cell with space group $I23$. Through the Rietveld analyses, the crystal structures have been determined, and they are the same as those reported by Jeitschko *et al* [18]. The lattice crystallographic data for $La_4Re_6O_{19}$ are listed in table 1. As shown in figure 2, the lattice parameters increase monotonically with the Ln^{3+} radius in ten-fold coordination. Figure 3 illustrates the schematic crystal structure of $Ln_4Re_6O_{19}$. The Re_2O_{10} units consist of two edge-sharing ReO_6 octahedra and the link to each other by sharing corners (see figure 3(a)). Lanthanide ions are inserted in the three-dimensional sequence of Re_2O_{10}. Furthermore, the oxide ion O(3), which is situated in a body-centred cubic position, is four-fold coordinated by lanthanide ions and the Ln_4O (Ln = La, Pr, Nd) tetrahedral cluster is formed as shown in figure 3(b). This cluster has no linkage to the other one.

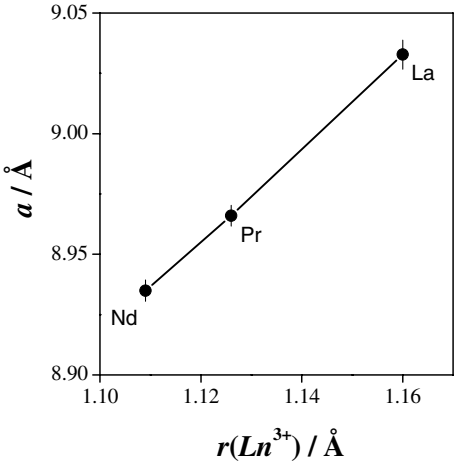

Figure 2. Variation of lattice parameters for $Ln_4Re_6O_{19}$ (Ln = La, Pr, Nd) with ionic radius of Ln^{3+}.

Table 1. Crystallographic, positional, occupational (g) and thermal (B) parameters for $La_4Re_6O_{19}$. (The definitions of the reliability factors R_I and R_{wp} are given as follows: $R_I = \sum |I_k(0) - I_k(c)| / \sum I_k(0)$ and $R_{wp} = [\sum w(|F(0)| - |F(c)|)^2 / \sum w(|F(0)|)^2]^{1/2}$.)

Space group $I23$ $a = 9.032(6)$ Å $R_I = 2.33\%$, $R_{wp} = 11.09\%$					
Atom	x	y	z	g	B (Å)
La	0.1597(1)	0.1597(1)	0.1597(1)	1.000	0.6(2)
Re	0.3668(1)	0.5	0	0.972(4)	0.1(2)
O1	0.681(2)	0	0	0.96(3)	0.9
O2	0.469(1)	0.169(1)	1.218(1)	0.97(2)	0.9
O3	0	0	0	1.000	0.9

The previous study reported that some vacancies existed at the Re site for only the Nd compound [17]. However, our present crystal structure analyses show that there exist no such defects for the La, Pr, and Nd compounds. Table 2 lists some selected interatomic distances for $La_4Re_6O_{19}$. The short Re–Re distance (~2.4 Å) in the Re_2O_{10} unit indicates a strong Re–Re bond.

3.2. Physical properties

3.2.1. $La_4Re_6O_{19}$. The temperature dependence of the magnetic susceptibilities for $La_4Re_6O_{19}$ is shown in figure 4. This compound exhibits Pauli paramagnetism, and the temperature-independent magnetic susceptibility is $\sim 4.5 \times 10^{-3}$ emu mol^{-1}. Below 15 K, Curie paramagnetism is observed, which is probably due to a small amount of impurities not detected in the x-ray diffraction measurement. For $La_4Re_6O_{19}$, because only the rhenium ion has unpaired electrons, the magnetic susceptibility measurement shows that the 5d electrons of the Re ion are delocalized.

Figure 5 shows the temperature dependence of the electrical resistivity (ρ) for $La_4Re_6O_{19}$. The electrical resistivity decreases monotonically with temperature and no anomaly is observed down to 0.35 K. In the case of a non-magnetic metallic conductor, the total resistivity (ρ) is defined by equation (1), and at high temperatures the phonon contribution (ρ_{ph}) to the electrical resistivity is proportional to temperature.

$$\rho(T) = \rho_0 + \rho_{ph}(T). \tag{1}$$

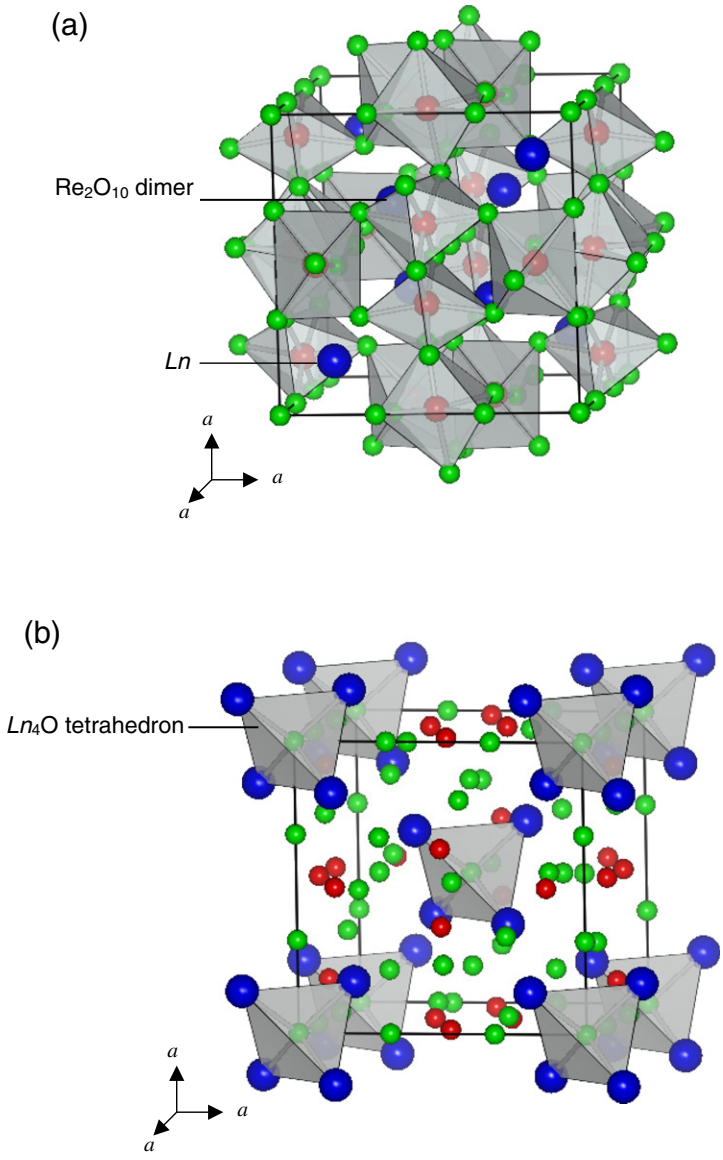

Figure 3. The crystal structure of $Ln_4Re_6O_{19}$ (Ln = La, Pr, Nd) compounds emphasizing (a) the three-dimensional net of Re_2O_{10} and (b) Ln_4O tetrahedra at body-centred cubic sites.

However, the temperature dependence of ρ_{ph} for $La_4Re_6O_{19}$ does not show any proportional relation. Therefore, supposing that the exponential part of T of the second term in equation (1) is n, we estimated n by fitting the following equation (2) to the experimental date over the temperature range 30–400 K:

$$\rho(T) = \rho_0 + AT^n. \tag{2}$$

The value of n was determined to be 1.39(1) (>1). This result is indicative of some contributions in addition to the phonon one (ρ_{ph}). As no magnetic contribution to the electrical resistivity exists owing to the absence of the localized magnetic moment, the resistivity with the temperature dependence of T^n ($n > 1$) may be derived from the resistivity by the scattering between conduction electrons or the thermal expansion with T^2 dependence, respectively, or

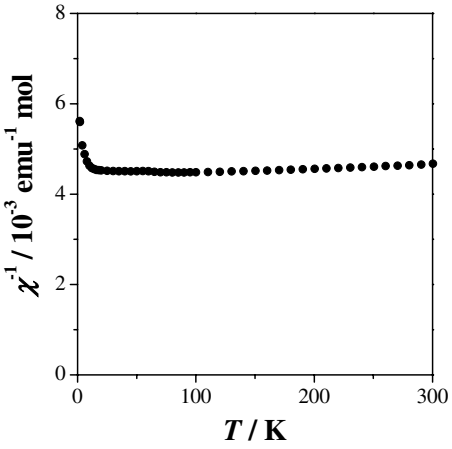

Figure 4. Temperature dependence of the molar magnetic susceptibility χ for $La_4Re_6O_{19}$.

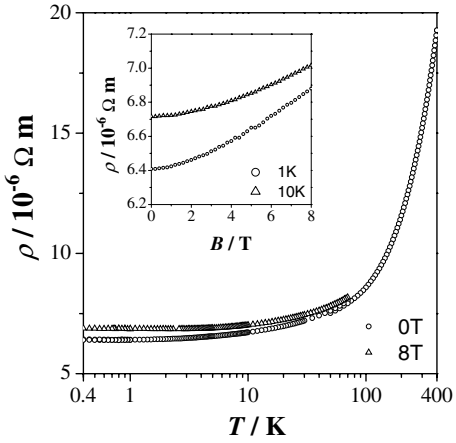

Figure 5. Temperature dependence of the electrical resistivity between 0.4 and 400 K at 0 and 8 T for $La_4Re_6O_{19}$. The inset shows the magnetic field dependence of the electrical resistivity measured at 1 and 10 K.

Table 2. Selected interatomic distances for $La_4Re_6O_{19}$.

ReO_6	Re–O1	2.030 Å × 2
	Re–O2	2.013 Å × 2
	Re–O2	2.053 Å × 2
Re_2O_{10}	Re–Re	2.407 Å
La_4O	O3–La	2.497 Å × 4
	La–La	4.078 Å × 6
LaO_{10}	La–O1	2.496 Å × 3
	La–O2	2.569 Å × 3
	La–O2	2.842 Å × 3
	La–O3	2.497 Å × 1

the resistivity by the sharpness of density of states at Fermi level, which is proportional to T^3 and T^4. This feature of resistivity for $La_4Re_6O_{19}$ is very similar to that of ReO_3 showing metallic behaviour [22].

The electrical resistivity as a function of the applied magnetic field is plotted in the inset of figure 5. The resistivity increases monotonically with magnetic field. It is recognized that

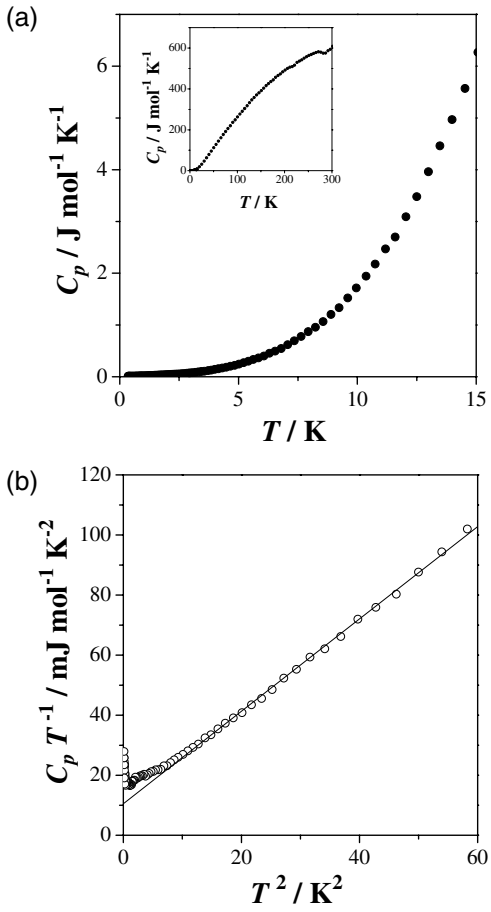

Figure 6. (a) The C_p versus T curve in the temperature range 0.35 K $\leqslant T \leqslant$ 15 K. The inset shows the C_p versus T curve in the range 0.35 K $\leqslant T \leqslant$ 300 K. (b) The C_p/T versus T^2 plot for $La_4Re_6O_{19}$. The solid line is the result of fitting with equation (3).

the magnetoresistance of $La_4Re_6O_{19}$ in high fields is almost linear to the magnetic field. For polycrystals, the average magnetoresistance in high fields is expected to be proportional to H, if the Fermi surface is 'open' [23].

Figure 6(a) shows the temperature dependence of the specific heat (C_p) in the temperature range 0.35 K $\leqslant T \leqslant$ 15 K. For $La_4Re_6O_{19}$, the total specific heat (C_p) consists of the lattice specific heat (C_{ph}) and electronic specific heat (C_{ele}). In the low temperature range, the total C_p can be represented by

$$C_p/T = \gamma + \beta T^2, \tag{3}$$

where β and γ are the lattice and electronic specific heat coefficients, respectively. By fitting equation (3) to the C_p/T–T^2 plot (see figure 6(b)), β and γ are obtained to be 1.539(6) mJ mol^{-1} K^{-4} and 10.6(3) mJ mol^{-1} K^{-2}, respectively. The Debye temperature Θ_D is estimated from the β value by

$$\Theta_D = (12\pi^4 nR/5\beta)^{1/3}, \tag{4}$$

where R is the gas constant. The Debye temperature Θ_D for $La_4Re_6O_{19}$ is 332.7(8) K. The small deviation of the C_p/T data from equation (3) at low temperatures may be attributable to a Schottky anomaly of nuclear spins of the Re nuclei [15, 24].

As mentioned above, the magnetic susceptibility, specific heat, and electrical resistivity measurements reveal that the delocalization of 5d electrons of the Re ion for $La_4Re_6O_{19}$

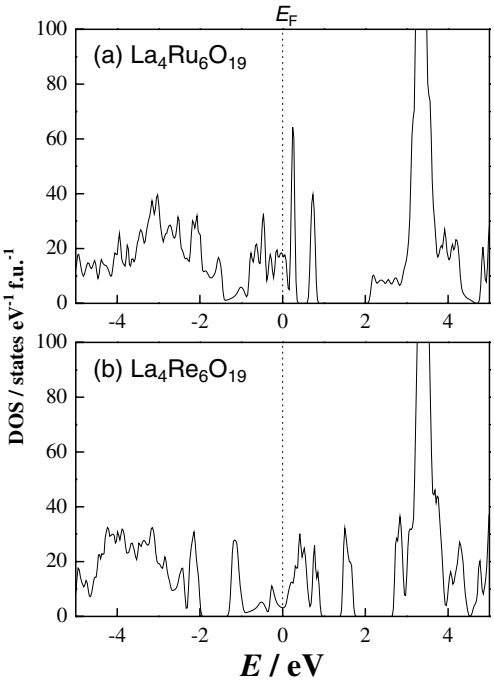

Figure 7. The total DOS plot for (a) $La_4Ru_6O_{19}$ and (b) $La_4Re_6O_{19}$. The Fermi level is at 0 eV in both plots.

results in the metallic nature. In the case of $La_4Ru_6O_{19}$, which has a non-Fermi-liquid characteristic, the 4d-orbital hybridization results from metal–metal bondings due to the short distance (∼2.5 Å) between the Ru ions in the Ru_2O_{10} dimer, which drives the opening of the band gap [15, 16]. This situation should cause unusual electronic properties. On the other hand, although $La_4Re_6O_{19}$ has a shorter Re–Re distance (∼2.4 Å) than the Ru–Ru (∼2.5 Å) distance in $La_4Ru_6O_{19}$, its physical properties show that $La_4Re_6O_{19}$ is a typical Fermi liquid.

In order to investigate the difference in the physical properties between $La_4Ru_6O_{19}$ and $La_4Re_6O_{19}$, calculations of the electronic structures have been performed for both $La_4Ru_6O_{19}$ and $La_4Re_6O_{19}$. Figure 7 shows the total DOS of $La_4Ru_6O_{19}$ and $La_4Re_6O_{19}$, respectively. The electronic structure of $La_4Ru_6O_{19}$ is very similar to that reported in figure 3 of [16]. On the other hand, it is revealed that $La_4Re_6O_{19}$ has a conduction band with a bandwidth of ∼2 eV near the Fermi level and that band gaps exist upper and below this conduction band. The DOS at the Fermi level is estimated to be 6.0 states eV^{-1} f.u.$^{-1}$ and the electronic specific heat coefficient (γ_{calc}) is calculated to be 7.5 mJ mol^{-1} K^{-1}. The mass enhancement parameter λ due to electron–electron correlations can be obtained from the ratio of

$$\frac{\gamma_{obs}}{\gamma_{calc}} = 1 + \lambda. \tag{5}$$

The value of λ is derived to be 0.4. This small value indicates that the electron–electron correlation is very weak in $La_4Re_6O_{19}$.

In $La_4Re_6O_{19}$, the rhenium ion is in the +4.33 oxidation state, i.e. one Re ion has 2.67 electrons in its t_{2g} orbitals. The three t_{2g} orbitals should hybridize to split into six hybrid states of σ, π, δ, δ^*, π^*, and σ^* character due to the effect of metal–metal bonding from an analogy with the molecular bonding scheme as given in figure 8(a). The shorter metal–metal bonding is expected to extend energy splittings of these hybrid states. The orbital-weighted bands of the t_{2g} orbitals are plotted in figure 8(c). The axis choice follows that in [16] (see figure 8(b)). For each Re_2O_{10} dimer, it is found that two Re $d_{x^2-y^2}$ orbitals give rise to σ and

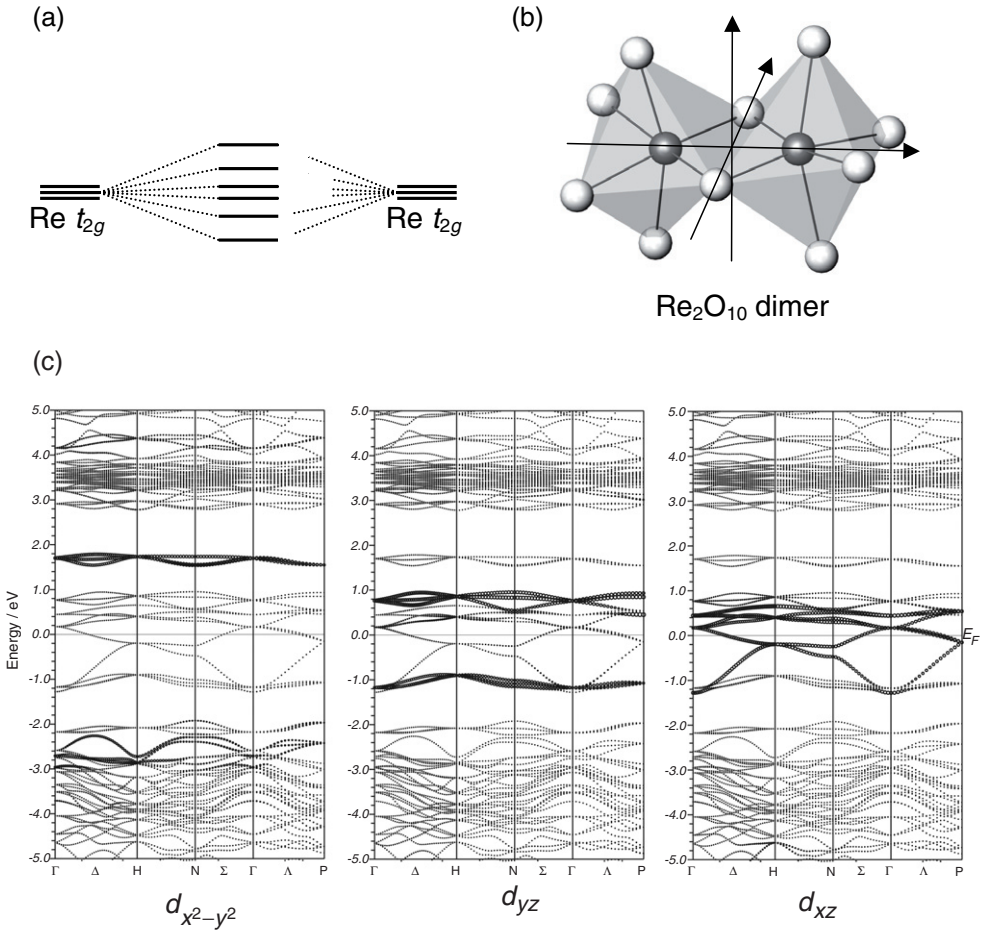

Figure 8. (a) Molecular orbital diagram of t_{2g} orbital hybridization between the Re ions in the Re_2O_{10} dimer. (b) Definition of the Re d-orbital directions following that in [16]. (c) Orbital-weighted bands of the t_{2g} orbitals for $La_4Re_6O_{19}$. The Fermi level is at 0 eV in all plots.

σ^* molecular orbitals. The Re d_{yz} and d_{xz} orbitals are also found to form π-type and δ-type molecular orbitals, respectively. Furthermore, the energy splittings between these σ-, π-, and δ-type orbitals are larger than those for $La_4Ru_6O_{19}$ reported in [16], which is attributable to the short Re–Re bonding. The calculations of the electronic structure for $La_4Re_6O_{19}$ reveal that the conduction band consists of π-type and δ-type orbitals originated from Re d_{yz} and d_{xz} orbitals and that this isolated band with lower degeneracy than that for $La_4Ru_6O_{19}$ causes a typical Fermi-liquid behaviour.

3.2.2. $Pr_4Re_6O_{19}$. Figure 9 and its inset show the temperature dependence of the reciprocal magnetic susceptibility and the magnetic susceptibility for $Pr_4Re_6O_{19}$, respectively. No evidence of any magnetic transition has been recognized down to 1.8 K. The reciprocal susceptibility exhibits Curie–Weiss behaviour above 50 K, but deviates from the Curie–Weiss law below 50 K. From the Curie–Weiss law fitting to the χ^{-1}–T curve in the temperature range 200–300 K, the effective magnetic moment ($\mu_{\rm eff}$) is obtained to be 3.60(1) $\mu_{\rm B}$. This value agrees well with the theoretical value of a free Pr^{3+} ion ($\mu_{\rm eff} = 3.58\ \mu_{\rm B}$; $g_J = 4/5$

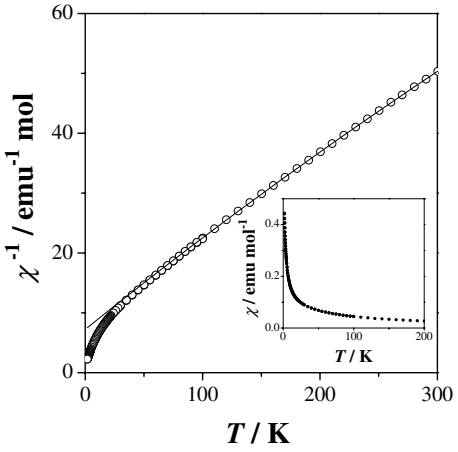

Figure 9. Temperature dependence of the reciprocal molar magnetic susceptibilities χ^{-1} for $Pr_4Re_6O_{19}$. The insets show the molar magnetic susceptibilities χ.

and $J = 4$), which indicates that the magnetic moment of the Re ion has no contribution to the effective magnetic moment for $Pr_4Re_6O_{19}$ and that the 5d electrons of the Re ion are delocalized. Consequently, the deviation from the Curie–Weiss law should be attributable to the crystalline electrical field (CEF) splitting of the nine-fold ground state ($^3H_4$) of the Pr^{3+} ion. Moreover, we calculated the Weiss constant (θ_W) by fitting the Curie–Weiss law to the χ^{-1}–T curve in the low temperature region (1.8 K $\leqslant T \leqslant$ 5 K). The negative Weiss constant ($\theta_W = -2.28(3)$ K) suggests that the magnetic exchange interaction is antiferromagnetic.

Figure 10(a) shows the temperature dependence of the specific heat (C_p) for $Pr_4Re_6O_{19}$. The C_p data on $La_4Re_6O_{19}$ are also plotted in the same figure. A broad maximum in the C_p versus T curve was observed around 2 K and the temperature of the maximum increases with the applied field. For $Pr_4Re_6O_{19}$, the total specific heat (C_p) consists of the lattice (C_{ph}), electronic (C_{ele}) and magnetic (C_{mag}) specific heat. On assuming that the lattice and electronic contributions to the total C_p are equal between $Pr_4Re_6O_{19}$ and $La_4Re_6O_{19}$, C_{mag} is obtained by subtracting the specific heat of $La_4Re_6O_{19}$ from that of $Pr_4Re_6O_{19}$. Figure 10(b) shows the C_{mag}/T–T curve of $Pr_4Re_6O_{19}$. The magnetic entropy change (S_{mag}) is calculated by the following equation:

$$S_{mag} = \int_0^T C_{mag}/T' \, dT'. \tag{6}$$

The value of S_{mag} per mole of Pr^{3+} ion ($\sim$5.5 J mol^{-1} K^{-1} at 15 K) is close to $R \ln 2$ ($\sim$5.8 J mol^{-1} K^{-1}). This result also indicates that the $^3H_4$ state of the Pr^{3+} ion is split by the CEF effect, so the ground state should be a doublet, or both the ground state and the first excited state are singlets. Below 1 K, an abrupt upturn is observed at 4 and 8 T, which may be attributable to a Schottky-type anomaly of nuclear spins for the Pr and/or Re nuclei.

In the case that the ground state is a doublet, the anomaly around 2 K is indicative of a long-range antiferromagnetic ordering of the Pr^{3+} moments. However, the large increase of the maximum temperature with the applied field denies the possibility of long-range antiferromagnetic ordering. On the assumption that both the ground state and the first excited state are singlets, the Schottky-type anomaly with the energy splitting of 4.5 K is plotted as a solid line in figure 10(b). It is seen that this Schottky-type curve differs considerably from the C_{mag}/T–T curve with zero field and that the C_{mag}/T–T curve has a tail of the magnetic specific heats up to 15 K. The sensitivity of this anomaly for the applied fields and the tail of the C_{mag}/T–T curve suggest that a short-range ordering exists among the Pr^{3+} moments. The

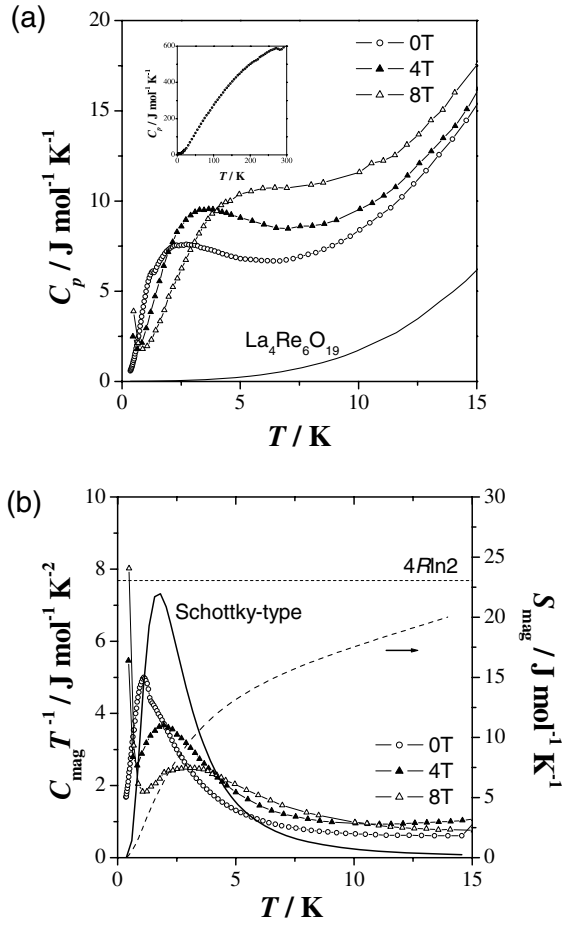

Figure 10. (a) The C_p versus T curves between 0.35 and 15 K at 0, 4 and 8 T for $Pr_4Re_6O_{19}$. The inset gives the C_p versus T curve measured in zero field between 0.35 and 300 K. The solid line indicates the C_p of $La_4Re_6O_{19}$. (b) The C_{mag}/T versus T curves at 0, 4 and 8 T (left ordinate) and the S_{mag} versus T curve at 0 T (right ordinate) for $Pr_4Re_6O_{19}$. The solid line is the estimated Schottky-type specific heat for the case of singlet ground and first excited states.

Pr ions form the Pr_4O cluster with an O3 ion and the arrangement of the Pr ions is a regular tetrahedron (see figure 3). It is considered that the Pr_4O clusters occupying the body-centred cubic sites cause a geometrically magnetic frustration without long-range ordering.

Figure 11 and its inset show the temperature and magnetic field dependence of the electrical resistivity (ρ) for $Pr_4Re_6O_{19}$, respectively. The temperature dependence of the electrical resistivity shows that this compound is metallic in electrical conductivity. For magnetic metals, the electrical resistivity consists of the residual resistivity (ρ_0), the phonon contribution (ρ_{ph}), and the magnetic contribution (ρ_{mag}) due to scatterings of conduction electrons by a fluctuation of magnetic moment. However, as shown in figure 11, both the temperature and the applied field dependences of the resistivity for $Pr_4Re_6O_{19}$ are quite similar to those for $La_4Re_6O_{19}$ (figure 5) and no remarkable magnetic contribution such as magnetic critical scatterings by the long-range ordering of the Pr^{3+} moments is observed. These results indicate that the ρ_{mag} contribution to the total ρ for $Pr_4Re_6O_{19}$ is small.

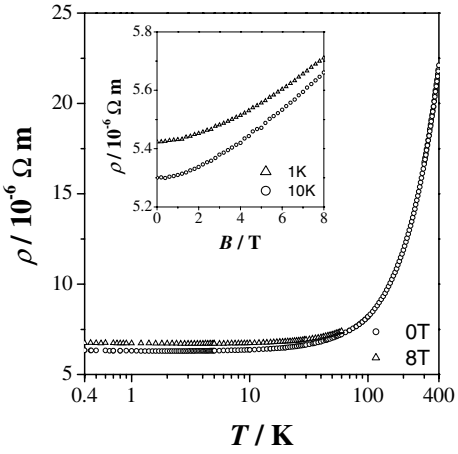

Figure 11. Temperature dependence of the electrical resistivity between 0.4 and 400 K at 0 and 8 T for $Pr_4Re_6O_{19}$. The inset shows the magnetic field dependence of the electrical resistivity at 1 and 10 K.

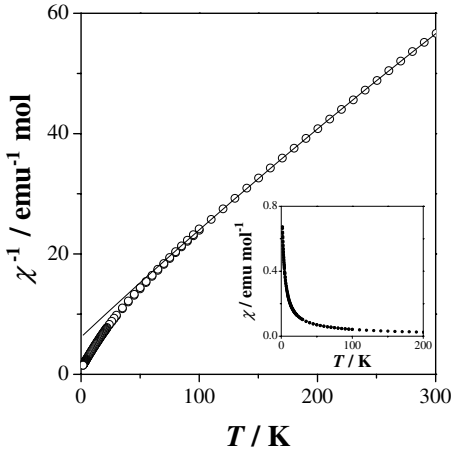

Figure 12. Temperature dependence of the reciprocal molar magnetic susceptibilities χ^{-1} for $Nd_4Re_6O_{19}$. The inset shows the molar magnetic susceptibilities χ.

3.2.3. $Nd_4Re_6O_{19}$. Figure 12 and its inset show the temperature dependence of the reciprocal magnetic susceptibility and the magnetic susceptibility for $Nd_4Re_6O_{19}$, respectively. No evidence of any magnetic transition has been recognized down to 1.8 K. The deviation from the Curie–Weiss law due to the CEF splitting is observed below 50 K. We calculated the effective magnetic moment ($\mu_{\rm eff}$) and the Weiss constant ($\theta_{\rm W}$) of the Nd^{3+} moment in the same manner as that for the Pr compound. The values obtained for $\mu_{\rm eff}$ and $\theta_{\rm W}$ are 3.60(2) $\mu_{\rm B}$ and $-2.68(6)$ K, respectively. The value of $\mu_{\rm eff}$ agrees well with the theoretical value of a free Nd^{3+} ion ($\mu_{\rm eff} = 3.62\ \mu_{\rm B}$; $g_J = 8/11$ and $J = 9/2$). In analogy with $Pr_4Re_6O_{19}$, these results suggest that the 5d electron of Re is delocalized and that antiferromagnetic interaction takes place for $Nd_4Re_6O_{19}$, also.

The temperature dependence of the specific heat ($C_{\rm p}$) of $Nd_4Re_6O_{19}$ is shown in figure 13(a). Two specific heat anomalies are observed under the zero-field condition; one is broad around 5 K and the other is sharp at 0.45 K. On increasing the applied magnetic field, the specific heat anomaly observed at 0.45 K under the zero-field condition moves to higher temperature (see arrows in figure 12(a)).

The magnetic contribution ($C_{\rm mag}$) to the total specific heat ($C_{\rm p}$) is estimated in the same manner as that for $Pr_4Re_6O_{19}$, and the $C_{\rm mag}/T$ versus T curve is shown in figure 13(b). In order

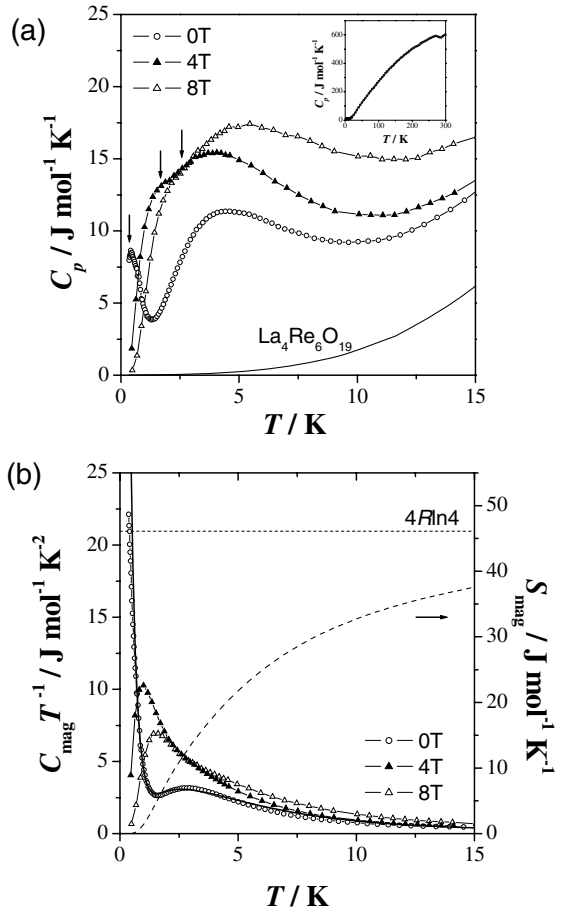

Figure 13. (a) The C_p versus T curves between 0.35 and 15 K at 0, 4 and 8 T for $Nd_4Re_6O_{19}$. Arrows indicate the lower temperatures at which the specific heat anomalies occur (see text). The inset gives the C_p versus T curve between 0.35 and 300 K at 0 T. The solid line indicates the C_p of $La_4Re_6O_{19}$. (b) The C_{mag}/T versus T curves at 0 and 4, 8 T (left ordinate) and the S_{mag} versus T curve at 8 T (right ordinate) for $Nd_4Re_6O_{19}$. The solid line is the Schottky-type specific heat estimated from the Nd energy levels.

to elucidate these two anomalies, the magnetic entropy change (S_{mag}) was calculated from the magnetic specific heat data by using equation (5). For the specific heats in zero field, because the sharp peak of the anomaly exists near the lowest limit of the measurable temperature, the change of S_{mag} at low temperatures cannot be estimated exactly. Therefore, S_{mag} was calculated from the C_{mag}/T data measured under the applied field of 8 T. The value of S_{mag} per mole of Nd^{3+} ion approaches $R\ln 4$ ($\sim$11.5 J mol^{-1} K^{-1}) as shown in figure 13(b). The $^4I_{9/2}$ ground state of the Nd^{3+} ion should split into five Kramers' doublets by the CEF effect in the low site symmetry of C_3 for the Nd ion coordinated by ten oxide ions. The change of S_{mag} below 15 K suggests that the ground and the first excited Kramers' doublets give rise to the anomalies at low temperatures.

The two anomalies at 0.45 K and around 5 K in the C_p–T curve seem to correspond to a long-range magnetic ordering and a Schottky-type anomaly, respectively. Figure 14(a) shows the C_{mag}/T versus T curve below 300 K. Another Schottky-type anomaly is observed

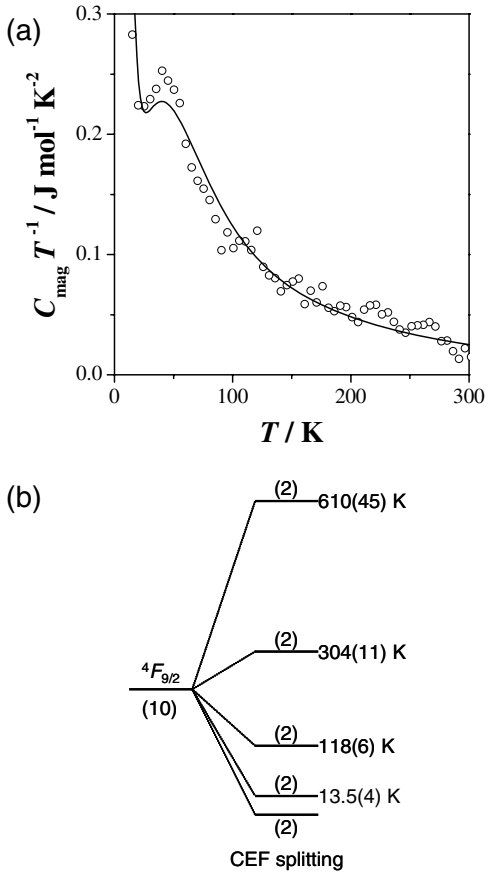

Figure 14. (a) The C_{mag}/T versus T curve below 300 K. A solid line is the Schottky-type specific heat estimated from the Nd energy levels. (b) The energy scheme of the CEF splitting for the Nd^{3+} ion in $Nd_4Re_6O_{19}$.

around 40 K. By using the C_{mag}/T curve measured under the zero-field condition, we have estimated the energy scheme of the CEF splitting derived from the $^4I_{9/2}$ state. The energy differences from the ground-state doublet were obtained to be 118(6) K for the second excited doublet, 304(11) K for the third excited doublet, and 610(45) K for the highest excited doublet, as shown in figure 14(b). This result means that the Schottky-type anomaly around 40 K is attributable to the second excited doublet and that these three excited states scarcely participate in the magnetic anomalies at low temperatures. For the ground and the first excited doublets, the C_{mag}/T curve at low temperatures could not be explained by using a simple Schottky-type model for a doublet–doublet system adapting the other excited doublets. However, it could be fitted by introducing the Zeemann splitting (splitting energy $\Delta \sim 11.7(8)$ K) of the first excited doublets where the energy difference between the ground state and the first excited state is 13.5(4) K. In the case of $Pr_4Re_6O_{19}$, the unusual broad specific heat around 2 K indicates the existence of short-range magnetic ordering. For $Nd_4Re_6O_{19}$, it is suggested that the Schottky-like anomaly around 5 K is attributable to the short-range magnetic ordering in the Nd_4O tetrahedral cluster and that the first excited state splits in the internal magnetic field (Zeemann splitting). Furthermore, the anomaly at 0.45 K is indicative of a long-range antiferromagnetic ordering between the Nd_4O tetrahedral clusters.

Figure 15(a) shows the temperature dependence of the electrical resistivity of $Nd_4Re_6O_{19}$ under zero field. The resistivity in zero field shows a monotonic increase in the temperature

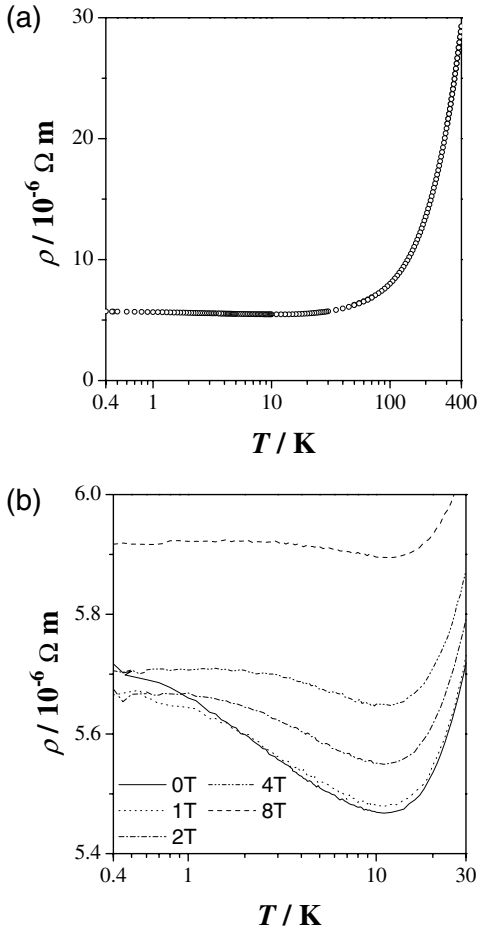

Figure 15. (a) Temperature dependence of the electrical resistivity between 0.4 and 400 K under zero field. (b) Temperature dependence of the electrical resistivity between 0.4 and 30 K at 0, 1, 2, 4, 8 T for $Nd_4Re_6O_{19}$.

range 10–400 K. $Nd_4Re_6O_{19}$ indicates a typical metallic behaviour similar to the case for $La_4Re_6O_{19}$ and $Pr_4Re_6O_{19}$. Figure 15(b) shows the temperature dependence of the electrical resistivity of $Nd_4Re_6O_{19}$ below 30 K under several applied magnetic fields. The resistivity below 10 K shows an upturn with decreasing temperature and this upturn is found to be suppressed by the applied field. It is considered that the anomaly below 10 K results from scatterings of conduction electrons by a fluctuation of the magnetic moment of Nd^{3+}, i.e. this phenomenon is 'a magnetic critical scattering' [25, 26], which is indicative of a long-range magnetic ordering. This result of the electrical resistivity measurement is consistent with the specific heat showing the long-range antiferromagnetic ordering at 0.45 K. The temperature of the long-range magnetic ordering is considerably lower than the onset temperature of the magnetic critical scattering ($\sim$10 K) for electrical resistivity and the Weiss constant (-2.68 K). Through the magnetic susceptibility, specific heat, electrical resistivity measurements for $Nd_4Re_6O_{19}$, it has been elucidated that the short-range magnetic orderings occur in the Nd_4O tetrahedral clusters much above the long-range ordering temperature and that the long-range ordering results from the magnetic interaction between the Nd_4O clusters via conduction electrons such as the Ruderman–Kittel–Kasuya–Yosida (RKKY) interaction.

4. Conclusion

All $Ln_4Re_6O_{19}$ (Ln = La, Pr, Nd) compounds have a cubic structure with space group $I23$ and show metallic behaviour owing to the delocalization of Re 5d electrons in the magnetic susceptibility, specific heat, and electrical resistivity measurements. This nature was also proved by the calculation of the electronic structure, which reveals that there exists weak electron–electron correlation.

For the compounds $Ln_4Re_6O_{19}$ (Ln = Pr, Nd), Schottky-type specific heat anomalies were observed at 2 K (Ln = Pr) and 5 K (Ln = Nd), which were due to the short-range magnetic ordering in the Ln_4O (Ln = Pr, Nd) tetrahedral cluster. In $Nd_4Re_6O_{19}$, long-range magnetic ordering through the conduction electrons of the Re ion was found at 0.45 K. The $Nd_4Re_6O_{19}$ compound shows unique behaviour involving the magnetic and electronic properties.

References

[1] Greedan J E, Reimers J N, Stager C V and Penny S L 1991 *Phys. Rev.* B **43** 5682
[2] Raju N P, Gmelin E and Kremer R K 1992 *Phys. Rev.* B **46** 5405
[3] Katsufuji T, Hwang H Y and Cheong S-W 2000 *Phys. Rev. Lett.* **84** 1998
[4] Taira N, Wakeshima M and Hinatsu Y 1999 *J. Solid State Chem.* **144** 216
[5] Wiebe C R, Gardner J S, Kim S-J, Luke G M, Wills A S, Gaulin B D, Greedan J E, Swainson I, Qiu Y and Jones C Y 2004 *Phys. Rev. Lett.* **93** 076403
[6] Taira N, Wakeshima M and Hinatsu Y 2001 *J. Phys.: Condens. Matter* **13** 5527
[7] Yanagishima D and Maeno Y 2001 *J. Phys. Soc. Japan* **70** 2880
[8] van Berkel F P F and IJdo D J W 1986 *Mater. Res. Bull.* **21** 1103
[9] Harada D and Hinatsu Y 2002 *J. Solid State Chem.* **164** 163
[10] Plaisier J R, Drost R J and IJdo D J W 2002 *J. Solid State Chem.* **169** 189
[11] Lam R, Langet T and Greedan J E 2003 *J. Solid State Chem.* **171** 317
[12] Nishimine H, Wakeshima M and Hinatsu Y 2004 *J. Solid State Chem.* **177** 739
[13] Hinatsu Y, Wakeshima M, Kawabuchi N and Taira N 2004 *J. Alloys Compounds* **374** 79
[14] Nishimine H, Wakeshima M and Hinatsu Y 2005 *J. Solid State Chem.* **178** 1221
[15] Khalifah P, Nelson K D, Jin R, Mao Z Q, Liu Y, Huang Q, Gao X P A, Ramirez A P and Cava R J 2001 *Nature* **411** 669
[16] Khalifah P and Cava R J 2001 *Phys. Rev.* B **64** 85111
[17] Bramnik K G, Abakumov A M, Shpanchenko R V, Antipov E V and van Tendeloo G 1998 *J. Alloys Compounds* **278** 98
[18] Jeitschko W, Heumannskämper D H, Schriewer-Pöttgen M S and Rodewald U Ch 1999 *J. Solid State Chem.* **147** 218
[19] Longo J M and Sleight A W 1968 *J. Inorg. Chem.* **7** 108
[20] Izumi F and Ikeda T 2000 *Mater. Sci. Forum* **321–324** 198
[21] Blaha P, Schwarz K, Madsen G K H, Kvasnicka D and Luitz J 2001 *WIEN2k, An Augmented Plane Wave Plus Local Orbitals Program for Calculating Crystal Properties* Vienna University of Technology, Austria (ISBN 3-9501031-1-2)
[22] King C N, Kisch H C and Geballe T H 1971 *Solid State Commun.* **9** 907
[23] Abrikosov A A 1988 *Fundamentals of the Theory of Metals* (Amsterdam: North-Holland)
[24] Tsuchida K, Kato C, Fujita T, Kobayashi Y and Sato M 2004 *J. Phys. Soc. Japan* **73** 698
[25] Hagen M, Child H R, Fernandez-Baca J A and Zarestky J L 1992 *J. Phys.: Condens. Matter* **4** 8879
[26] Sato N, Aso N, Hirota K, Komatsubara T, Endoh Y, Shapiro S M, Lander G H and Kakurai K 1996 *Phys. Rev.* B **53** 14043